

Contents lists available at ScienceDirect

Heliyon

journal homepage: www.cell.com/heliyon



Research article



Yishen Huashi granule modulated lipid metabolism in diabetic nephropathy via PI3K/AKT/mTOR signaling pathways

Tingting Zhao ^{a,1}, Qian Xiang ^{a,1}, Beifeng Lie ^{b,1}, Deqi Chen ^b, Minyi Li ^b, Xi Zhang ^a, Junzheng Yang ^b, Bao He ^b, Wei Zhang ^a, Ruixue Dong ^c, Yadi Liu ^a, Junling Gu ^a, Quan Zhu ^b, Yijing Yao ^a, Tingting Duan ^{b,***}, Zhenghai Li ^{b,**}, Youhua Xu ^{a,c,d,e,*}

- ^a Faculty of Chinese Medicine, State Key Laboratory of Quality Research in Chinese Medicines, Macau University of Science and Technology, Taipa, Macao, PR China
- ^b Institute of Consun Co. for Chinese Medicine in Kidney Diseases, Guangdong Consun Pharmaceutical Group, Dongpeng Road 71, Guangzhou, PR China
- ^c School of Pharmacy, State Key Laboratory of Quality Research in Chinese Medicines, Macau University of Science and Technology, Taipa, Macao, PR China
- ^d Department of Endocrinology, Zhuhai Hospital of Integrated Traditional Chinese and Western Medicine, Zhuhai, PR China
- e Macau University of Science and Technology Zhuhai MUST Science and Technology Research Institute, Hengqin, Zhuhai, PR China

ARTICLE INFO

Keywords: Diabetic nephropathy Lipid metabolism Yishen Huashi Intestinal-liver axis

ABSTRACT

Aim: Diabetic nephropathy (DN) is the primary cause of end-stage renal disease worldwide. Although etiology for DN is complex and still needs to be fully understood, lipid metabolism disorder is found to play a role in it. Previously, we found Yishen Huashi (YSHS) granule could inhibit diabetic damage and reduce level of microalbuminuria (mALB) in DN animals. To explore its role and mechanism in lipid metabolism under DN settings, this study was designed.

Materials and methods: DN rats were induced by streptozotocin (STZ), HepG₂ and CaCO₂ cells were applied for *in vitro* study. Hematoxylin-Eosin (HE), periodic acid–Schiff (PAS) staining, and Transmission Electron Microscopy (TEM) were applied for histological observation; 16s Sequencing was used for intestinal microbiota composition analysis; western blotting (WB) and immunofluorescence were carried out for molecular biological study, and enzyme-linked immunosorbent assay (ELISA) was used for lipid determination.

Results: YSHS administration significantly reduced levels of total cholesterol (TC), triglyceride (TG), and low-density lipoprotein (LDL-C), while increased level of high-density lipoprotein (HDL-C); meanwhile, histological changes and steatosis of the liver was ameliorated, integrity of the intestinal barrier was enhanced, and dysbacteriosis within intestinal lumen was ameliorated. Mechanism study found that YSHS modulated mitophagy within hepatocytes and inhibited mTOR/AMPK/PI3K/AKT signaling pathway.

Conclusion: In conclusion, we found in the present study that YSHS administration could ameliorate lipid metabolism disorder in DN animals, and its modulation on intestinal-liver axis played a significant role in it.

^{*} Corresponding author. Faculty of Chinese Medicine, State Key Laboratory of Quality Research in Chinese Medicines, Macau University of Science and Technology, Taipa, Macao, PR China.

^{**} Corresponding author.

^{***} Corresponding author.

E-mail addresses: duantt@chinaconsun.com (T. Duan), lizh@chinaconsun.com (Z. Li), xuyouhua_021@163.com, yhxu@must.edu.mo (Y. Xu).

 $^{^{1}}$ Contributed equally to the work.

1. Introduction

Diabetic nephropathy (DN) is a common microvascular complication of diabetes. Due to limited treatment strategy, it is still a common cause of chronic kidney disease [1]. The progression of DN is caused by structural and functional changes caused by hemodynamic and metabolic changes [2], and modulating lipid metabolism is indicated to play a role in inhibiting progression of DN.

Liver plays an important role in fat metabolism [3–5]. However, its function is severely damaged in DN [6]. It is reported that hyperglycemia glycosylates apolipoprotein and increases fat accumulation within hepatocytes [7]. Insulin resistance (IR) accompanied with low-grade inflammation is a characteristic of diabetes and its complication, including DN. It was reported that IR is closely related with obesity and hyperlipidemia [8], and inflammation will significantly deteriorate IR-induced syndromes. Although source of inflammation under diabetic settings is still not fully understood, gut-leak is believed to be a non-negligible factor [9]. It is found that diabetes and DN will influence the expression and function of tight junction protein in the intestinal mucosa epithelium [10,11], lead to increased permeability of the intestinal wall, and result in persistent low-level inflammation in patients with DN. In this view, gut-liver axis is supposed to ameliorate lipid metabolism disorder as well as DN [12]. Previously, we have demonstrated that supplementation with metabolite short chain fatty acids is help to improve liver metabolism [13], suggesting modulating gut-liver axis may help to modulate lipid metabolism.

Yishen Huashi (YSHS) granule is a prescription drug approved by China Food and Drug Administration (CFDA) in the year 2009 (No. Z20090250) to treat kidney disease. Deriving from "Shengyang Yiwei Decoction", YSHS is composed of 16 traditional Chinese medicines such as Ginseng (Ren Shen in Chinese) and Astragali Radix (Huang Qi in Chinese). Previously, we found oral administration with extract from Astragali Radix had protective effect against diabetes and its accompanied gut-leak [14]. A series of active component from YSHS was found to inhibit progression of diabetes and DN [15,16]. Besides that, we also found Calycosin from Astragali Radix could modulate glucose uptake in hepatocyte [17]. Based on its definite clinical effect on kidney, an expert consensus was released in 2020 [18]. Microalbuminuria (mALB) [19] is widely recognized as the earliest marker of DN. Most recently, we found oral administration with YSHS has significant effect on decreasing mALB by preserving integrity of glomerular filtration barrier [20]. However, the influence of YSHS on lipid metabolism is still waiting to be explored.

Clinically, YSHS is orally administrated. PI3K/Akt/mTOR is a classic signaling pathway found to be highly expressed in DN, and the blockade of these pathways may slow the progression and development of DN [21]. Concerning pivotal role of gut-liver axis in DN, the present study was designed, and both *in vivo* and *in vitro* studies were carried out. Findings in this study supplied an idea on exploring effect of Chinese Medicines and is also help to understand mechanism of YSHS on ameliorating DN.

2. Materials and methods

2.1. Yishen Huashi (YSHS) qualification

The details about the herbs of YSHS used in this study were described in Table 1. YSHS (batch number: 20201101) were produced and provided by Consun (Guangzhou, China), and its quality was verified by Q-TOF (Fig. 1). According to Chinese pharmacopoeia [22], the preparation process of YSHS was as follows: Panax ginseng C.A.Mey. 170.5 g, Astragalus membranaceus (Fisch.) Bunge 341 g, Poria cocos (Schw.) Wolf 51.1 g, Ziziphus jujuba Mill. 100 g, Pinellia ternata (Thunb.) Makino 170.5 g, Glycyrrhiza uralensis Fisch. 170.5 g, Notopterygium incisum K.C.Ting ex H.T.Chang 85.2 g, Angelica pubescens Maxim. 85.2 g, Saposhnikovia divaricata (Turcz.) Schischk. 85.2 g, Cynanchum otophyllum C.K.Schneid. 85.2 g, Citrus reticulata Blanco 68.2 g, Atractylodes macrocephala Koidz. 51.1 g, Alisma plantago-aquatica L. 51.1 g, Bupleurum chinense DC. 51.1 g, Zingiber officinale Roscoe 50 g, and Coptis chinensis Franch 34.1 g; herbal

Table 1 Herbs in Yishen Huashi granule.

Botanical name	English name	Chinese name	Used part	Lot No.	Batch number
Astragalus membranaceus (Fisch.) Bunge	Astragalus membranaceus	Huang Qi	Root	20200421	20201101
Panax ginseng C.A.Mey.	Ginseng Root	Ren Shen	Rhizomes and roots	20200428	20201101
Pinellia ternata (Thunb.) Makino	Ternate Pinellia	Ban Xia	Tubers	20200424	20201101
Glycyrrhiza uralensis Fisch.	Baked licorice	Zhi Gan Cao	Rhizomes and roots	20200434	20201101
Ziziphus jujuba Mill.	Common Jujube	Da Zao	Fruit	20200427	20201101
Notopterygium incisum K.C.Ting ex H.T.	Incised Notopterygium	Qiang Huo	Rhizomes and roots	20200435	20201101
Chang					
Angelica pubescens Maxim.	Root of Doubleteeth Pubescent Angelica	Du Huo	Root	20200430	20201101
Saposhnikovia divaricata (Turcz.) Schischk.	Divaricate Saposhniovia Root	Fang Feng	Root	20200429	20201101
Cynanchum otophyllum C.K.Schneid.	White peony root	Bai Shao	Root	20200531	20201101
Citrus reticulata Blanco	Tangerine Peel	Chen Pi	Pericarp	20200426	20201101
Atractylodes macrocephala Koidz.	Largehead Atractylodes Rhizome	Bai Zhu	Rhizome	20200431	20201101
Poria cocos(Schw.) Wolf	Indian Buead Tuckahoe	Fu Ling	Dried sclerotia	20200422	20201101
Alisma plantago-aquatica L.	Oriental Waterplantain Tuber	Ze Xie	Tubers	20200423	20201101
Bupleurum chinense DC.	Chinese Thorawax Root	Chai Hu	Root	20200432	20201101
Zingiber officinale Roscoe	Ginger	Sheng Jiang	Rhizome	20200438	20201101
Coptis chinensis Franch.	Coptis chinensis	Huang Lian	Rhizome	20200433	20201101

The plant name has been checked with http://www.theplantlist.org.

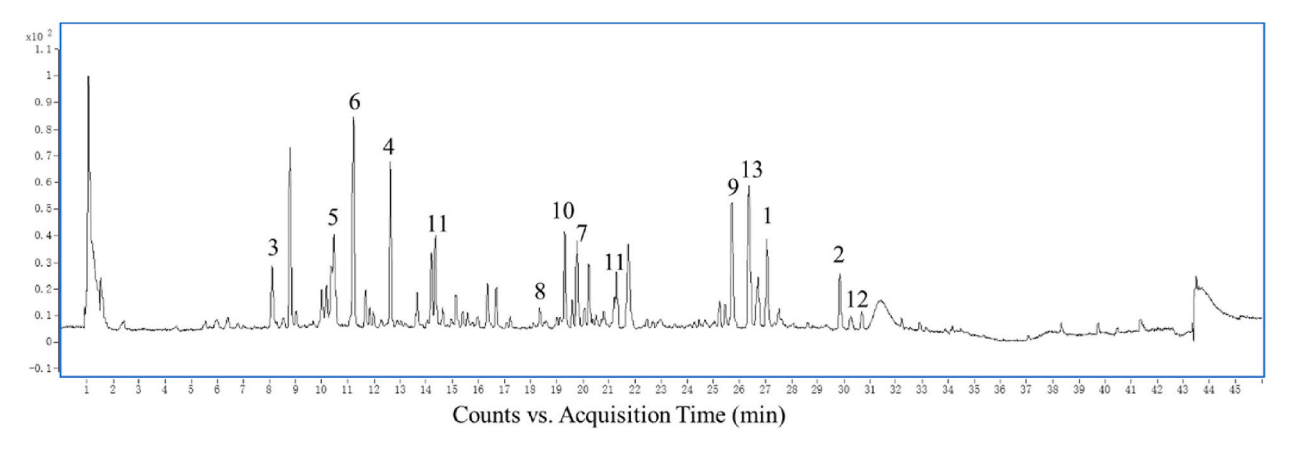


Fig. 1. Quality Control of YSHS. Q-TOF Mass Spectrometer chromatogram of YSHS as well as its major components including 1. Berberine; 2.10-Gingerol; 3. Alisol B 23-acetate; 4. Hesperidin; 5. Paeoniflorin Paeoniflorin; 6. Calycosin-7-O-β-D-glucoside; 7. Columbianadin; 8. Isoimperatorin; 9. Notopterol; 10. Ginsenoside Rb1; 11. Ginsenoside Re; 12. Ginsenoside Rg1; 13. Astragaloside IV.

medicines were exposed to water; then the sample was heated, boiled and refluxed for 3 times; finally, the extract was filtered and concentrated at $60\,^{\circ}$ C to $1000\,$ g.

2.2. Animals

Male Wistar rats (180–220 g) were derived from Guangdong Medical Laboratory Animal Center. DN was induced with streptozotocin (STZ; 30 mg/kg i.p.) once a week for three consecutive weeks. Blood glucose was measured 24 h after the last STZ injection. And urine microalbumin was measured to accumulate data (Supplementary Table S1). Rats were considered to have DN when the fasting blood glucose level exceeded 16–30 mmol/L and with high level of mALB. DN rats were divided into 4 groups with 6 in each group: DN rats were orally administrated with YSHS (low dose, 1.3 g/kg/day; medium dose, 2.7 g/kg/day; high dose, 5.4 g/kg/day) or Irbesartan (IRB; 27 mg/kg) daily for eight consecutive weeks. The animals were then anesthetized, and samples were collected. All animal care and experimental design was approved by Macau University of Science and Technology (Approval no. AL018/DICV/DIS/2019).

2.3. Hematoxylin-Eosin (HE) and periodic acid-Schiff (PAS) staining

The liver was fixed in 10% buffered formalin for histological and immunohistological examination. Tissues were blocked in paraffin and sectioned at $5 \mu m$ thickness for HE and PAS examination.

2.4. Transmission Electron Microscopy (TEM)

Liver and intestinal tissues were cleaved into 1 mm³ cubes with a cold blade and fixed with 4% glutaraldehyde. Tissues were fixed with 1% OsO₄, dehydrated with graded acetone, permeated with epoxy resin, embedded, sectioned, and finally stained with uranyl acetate and lead citrate. Slices were observed by TEM.

2.5. 16s sequencing

Total genome DNA from samples was extracted by CTAB/SDS method. DNA concentration and purity was monitored on 1% agarose gels. 16S rRNA/18SrRNA/ITS genes of distinct regions (16S V4/16S V3/16S V3-V4/16S V4-V5, 18S V4/18S V9, ITS1/ITS2, Arc V4) were amplified using specific primer (e.g., 16S V4: 515F-806R, 18S V4: 528F-706R, 18S V9: 1380F-1510R, et al.) with the barcode. All PCR reactions were carried out with 15 μ L of Phusion® High-Fidelity PCR Master Mix (New England Biolabs). PCR products were electrophoresized on 2% agarose gel for detection. And mixture PCR products was purified with Qiagen Gel Extraction Kit (Qiagen, Germany). Sequencing libraries were generated using TruSeq® DNA PCR-Free Sample Preparation Kit (Illumina, USA) following manufacturer's instruction. The library quality was assessed on the Qubit 2.0 Fluorometer (Thermo Scientific) and Agilent Bioanalyzer 2100 system. At last, the library was sequenced on an Illumina NovaSeq platform and 250 bp paired-end reads were generated.

2.6. Cell culture

 $HepG_2$ and $CaCO_2$ cells were purchased from American Type Culture Collection (ATCC) (Manassas, VA). $HepG_2$ cells were cultured in high-glucose MEM medium (Gibco) supplemented with 10% fetal bovine serum (FBS) and 1% penicillin-streptomycin (PS) at 37 °C in the incubator. $CaCO_2$ cells were cultured in high-glucose DMEM medium (Gibco) supplemented with 10% FBS, 1% glutamine, 1%

non-essential amino acid and 1% penicillin-streptomycin at 37 °C in the incubator.

2.7. Cell counting kit-8 (CCK8) assay

A CCK8 kit (Beyotime, Shanghai, China) was used to assess cell proliferation. Cells were re-suspended and seeded into 96-well plates at a density of 1×10^4 cells per well. The plates were incubated at 37 °C for 1.5 h. The absorbance value at OD 490 nm were measured using a plate reader.

2.8. Determination of mitochondrial DNA copy number

Mitochondrial DNA copy number was determined by Real-time PCR [23]. The mitochondrial DNA copy number is the numerical value of the mitochondrial minor arc (MinArc) content corrected for the nuclear single-copy β -2 microglobulin (β 2M) content in the mitochondria. The contents of MinArc and β 2M were determined by Real-time PCR, primers sequences shown in Table 2. Mitochondrial and genomic DNA within cells were extracted by QIAamp® DNA Micro Kit according to protocol supplied by the supplier. DNA concentration of the samples was measured with NanoDrop spectrophotometer, and quantified to 10 ng/ μ L for subsequent Q-PCR. Q-PCR reaction was took place on ViiATM7 (Life Technologies, Gaithersburg, MD, USA) System according to the supplier's protocol. The $2^{-\triangle\triangle}$ Ct method was used to calculate the relative mitochondrial DNA copy number.

2.9. Western blotting (WB)

Total proteins were extracted by RIPA. Proteins were separated by SDS-PAGE and electro-transferred onto PVDF membranes. The membranes were soaked in buffer containing 5% BSA for 1 h and then incubated with primary antibodies including anti-p-mTOR (5536s, 1:1000, Cell Signaling Technology), anti-p-PI3K (bs-6417R, 1:1000, Bioss), anti-PI3K (bs-10657R, 1:1000, Bioss), anti-p-AMPK (2531S, 1:1000, Cell Signaling Technology), anti-AMPK (5832S, 1:1000, Cell Signaling Technology), anti-PAMPK (5832S, 1:1000, Cell Signaling Technology), anti-PAKT (Sc-293125, 1:1000, Santa), anti-AKT (Sc-5298, 1:1000, Santa), anti-PGC1 α (bs-7535R, 1:1000, Bioss), anti-LC3B (ab51520, 1:5000, Abcam), anti-ZO-1 (61–7300, 1:1000, Invitrogen), anti-Occludin (71–1500, 1:1000, Invitrogen), or anti-Claudin-5 (34–1600, 1:1000, Invitrogen), at 4 °C overnight. Thereafter, the membranes were washed with Trisbuffered saline Tween buffer and incubated with HRP-rabbit (ab191866, 1:5000, Abcam) or HRP-mouse (bs-0296G-HRP, 1:1000, Bioss) conjugated secondary antibody for 1 h at room temperature (RT). An Odyssey Infrared Imaging System was used to scan the membranes for further analysis. β -actin (CL594-66009, 1:1000, Proteintech) was used as loading control. Band intensities were quantified using Image J software.

2.10. Immunofluorescence

 ${\rm HepG_2}$ or ${\rm CaCO_2}$ cells were plated onto coverslips and incubated with drugs for 24 h after being cultivated overnight. Cells were fixed with 4% paraformaldehyde solution and permeabilized with 0.5% Triton X-100 PBS solution. After washing with PBS, unspecific binding sites were blocked with 5% BSA for 60 min at RT. Then, cells were incubated with primary antibody overnight at 4 °C. After washing three times with PBS, cells were incubated with secondary antibody (bs-0369m-FITC Mouse Anti-Rabbit IgM/FITC, or bs-0296G-Cy3 Goat Anti-Mouse IgG/Cy3; 1: 200) for 1 h in the dark at RT. Nuclei were counter-stained by DAPI (D3571, 1:200, Invitrogen) for 5 min at RT. Images of the staining were taken with a confocal laser scanning microscopy (Leica TCS SP8, Germany) under standardized conditions and analyzed with Image J software.

2.11. Enzyme-linked reaction

Levels of total cholesterol (TC; A111-1-1, Nanjing Jiancheng, China), triglyceride (TG; A110-1-1, Nanjing Jiancheng, China), high density lipoprotein cholesterol (HDL-C; A112-1-1, Nanjing Jiancheng, China), low density lipoprotein cholesterol (LDL-C; A113-1-1, Nanjing Jiancheng, China), alaninetransaminase (ALT; C009-2-1, Nanjing Jiancheng, China), and alaninetransaminase (AST; C010-2-1, Nanjing Jiancheng, China) were measured with the microplate test kits according to the manufacturer's instructions.

2.12. Statistical analysis

All results are presented in the format of mean \pm standard error of the mean (SEM). Data were analyzed using one-way analysis of variance (ANOVA). P < 0.05 was considered statistically significant. All statistical analyses were performed with GraphPad prism 7.00 for Windows.

 Table 2

 List of sequences for primers used in PCR analysis.

Gene	Forward primers (5′–3′)	Reverse primers (5′–3′)
MinArc	CTAAATAGCCCACACGTTCCC	AGAGCTCCCGTGAGTGGTTA
β2M	GCTGGGTAGCTCTAAACAATGTATTCA	CCATGTACTAACAAATGTCTAAAAATGGT

3. Results

3.1. YSHS modulated lipid metabolism in DN rats

Liver plays a pivotal role in modulating lipid metabolism. In the present study, as shown in Fig. 2A, we found the liver index in Irbesartan (Irb) and YSHS groups was lower than that in the DN group; moreover, serum levels of TC, TG, and LDL-C were significantly reduced by YSHS in DN animals (Fig. 2B–D). We also observed the elevated levels of ALT and AST in DN animals were decreased by YSHS administration (Fig. 2E and F). As YSHS at middle dose showed more significant effects on lipid metabolism, this dose was applied in the following study.

To confirm the efficacy of YSHS in protecting liver function in STZ-exposed rats, histological changes of related organs were observed with light microscopy as well as TEM. As shown in Fig. 3A, the structure of the liver lobules in the normal group is clear, and the hepatocyte cords are neatly arranged. In DN rats, the liver lobule structure is disordered, a large number of small vacuoles can be seen in the cytoplasm of hepatocytes; in some cells, multiple small vacuoles are fused into large vacuoles. While in YSHS or Irb treatment groups, the structure of the liver lobules was clearer, and the intra-cytoplasmic vacuoles of hepatocytes were significantly reduced. To observe glycogen synthesis within hepatocytes, PAS staining was carried out. Rich purple-red glycogen particles can be seen in the cytoplasm of the hepatocytes in normal rats, especially in the area near the portal duct of the liver lobules; while glycogen particles in the hepatocytes of the DN group were decreased or even disappeared, and YSHS or Irb administration significantly increased its content compared with DN group (Fig. 3B). This was verified by TEM observation that the hepatocyte nucleus in DN animals was constricted, the cytoplasm contained a large number of lipid droplets, most of the lipid droplets were fused, the organelles were significantly reduced, collagen fibers were proliferated, and intrahepatic cholestasis was accompanied by the formation of myelin-like bodies; while in YSHS or Irb treatment group, the hepatocyte nucleus constriction was significantly reduced, the lipid droplets in the cytoplasm were reduced, the fat storage cells were reduced, and the intrahepatic cholestasis was significantly reduced (Fig. 3C).

Considering YSHS was orally administrated and intestinal tract plays key role in substance absorption and metabolism, its structure was firstly observed by TEM. We observed in DN rats that the intestinal epithelial cell space was enlarged, the microvilli were thick and short, the intercellular connections were disordered, there was obvious tissue edema, and the macrophages were enlarged in volume, irregular in shape, and showed activation; on the other hand, YSHS administration significantly ameliorated the abnormal structure in that the intercellular junction structure of the intestinal lumen was enhanced, the microvilli were neat, and the macrophage morphology was regular (Fig. 3D).

The above findings suggested that YSHS administration could modulate lipid metabolism in DN animals, and its protection on liver and intestine function may play a role.

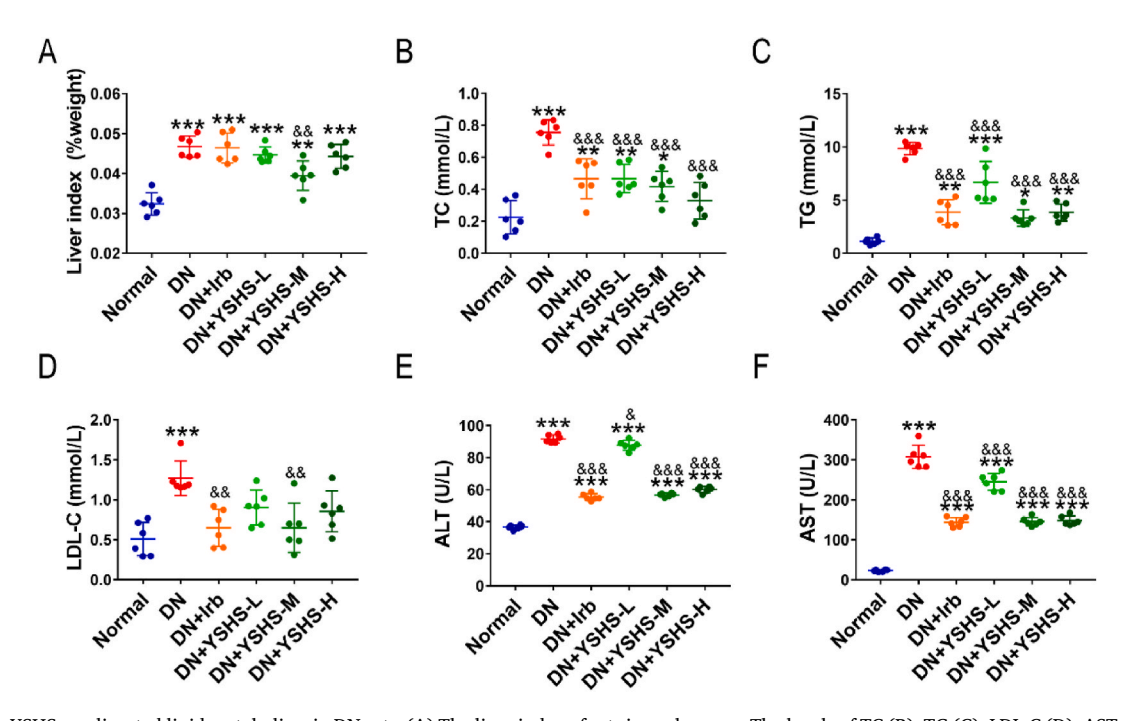


Fig. 2. YSHS ameliorated lipid metabolism in DN rats. (A) The liver index of rats in each group. The levels of TC (B), TG (C), LDL-C (D), AST (E), and ALT (F) in each group was determined by the Elisa kit. *p < 0.05, **p < 0.01, ***p < 0.001, vs. Normal; *p < 0.05, *&*p < 0.01, *&**p < 0.001, vs. DN.

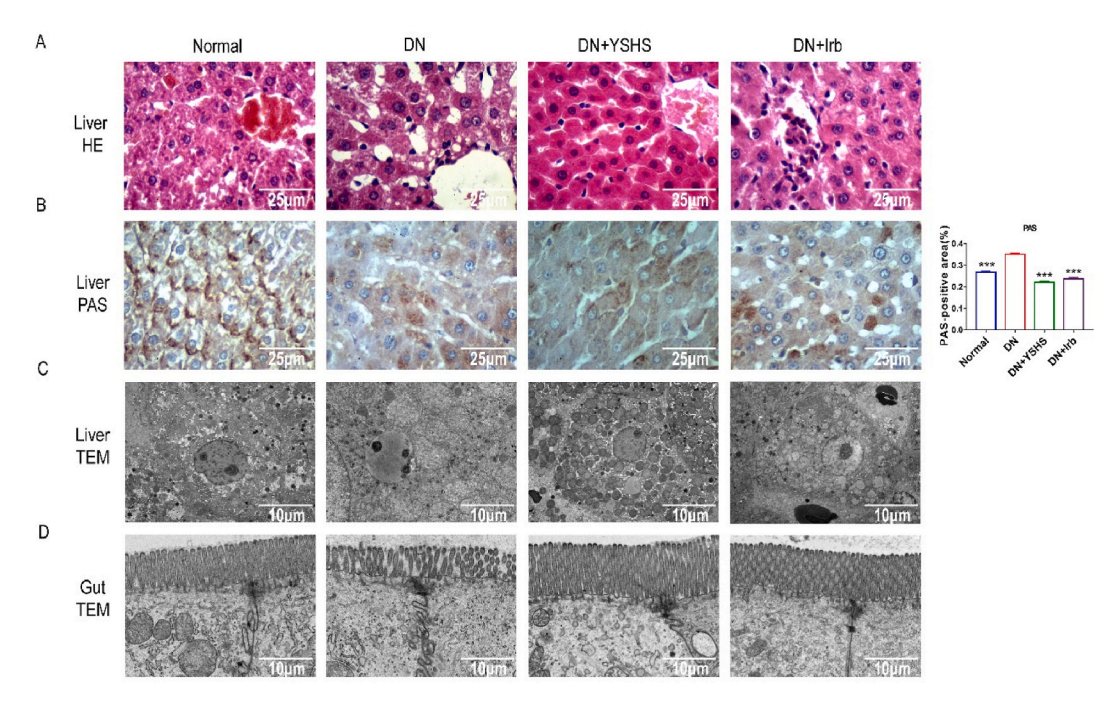


Fig. 3. YSHS ameliorated abnormal histology in DN rats. (A) H&E staining of liver tissues. (B) PAS staining of liver tissues and its statistics. (C) Transmission electron microscope of liver tissues. (D) Transmission electron microscope of gut tissues.

3.2. YSHS ameliorated mitophagy in DN rats

Mitochondria dysfunction has been demonstrated to play a pivotal role in metabolism and development of DN. Since PGC-1 α is a major metabolic regulator in mitochondrial homeostasis, we were interested in elucidating the role of this co-activator in mitochondrial removal by mitophagy. In the present study, we observed DN significantly inhibited PGC-1 α expression in the liver, and this reduction was reversed by YSHS administration (Fig. 4A and D). LC3 is a well-established marker of autophagosomes in mammalian cells. When autophagy occurs, punctate LC3 protein appears, and the soluble form of LC3 (LC3-I) is converted into the lipidated and autophagosome-associated form (LC3-II). In the present study, WB analysis indicated that the expression of both LC3-I and LC3-II

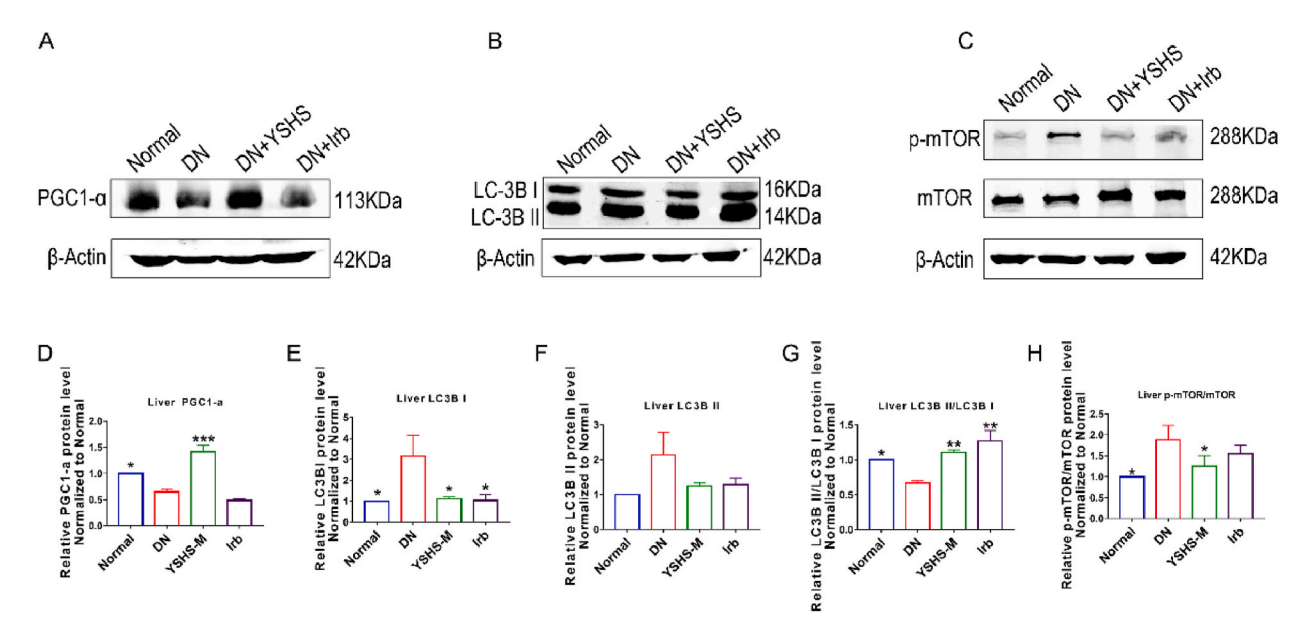


Fig. 4. YSHS ameliorated mitophagy in DN rats. WB detection of PGC1- α (A) and LC3B (B) proteins; (C) WB detection of *p*-mTOR and total mTOR; ratio of PGC1- α (D), LC3BI (E) and LC3BII (F); ratio of LC3BII/LC3BI (G); ratio of *p*-mTOR/mTOR (H). *p < 0.05, **p < 0.01, ***p < 0.001, vs. DN.

proteins were increased in DN liver, YSHS significantly reduced LC3-I and LC3-II puncta formation (Fig. 4B,E,F), the level of autophagy was significantly increased by YSHS (Fig. 4G), and the mTOR-related signaling pathway contributed to autophagy in the liver (Fig. 4C, H).

3.3. YSHS modulated composition of intestinal flora in DN rats

We have observed YSHS administration preserved integrity of the intestinal structure in DN rats (Fig. 3D). Since imbalance of gut flora contributes to intestinal barrier injury, we carried out 16s ribosomal RNA (rRNA) sequencing. Rank abundance plot, Venn analysis, and Ternary phase diagram revealed significant changes of Operational Taxonomic Unit (OUT) among groups (Fig. 5A–C), and the species relative abundance histogram comparison exhibited different diversity in DN rats (Fig. 5D), indicating a significant dysbacteriosis in DN rats. Genus-level species tree was shown in Fig. 5E. And heatmap analysis verified multiple alterations of bacterial flora at the species level, among which *Proteobacteria*, *Desulfobacterota*, *Acidobacteriota*, *Kapabacteria*, *Myxococcota*, *Chloroflexi*, *Nitrospirota*, *Bdellovibrionota*, *Zixibacteria*, *Spirochaetota*, and *SAR324_clade* (*Marine_group_B*) population were increased, while *Firmicutes*, *Bacteroidota*, *Verrucomicrobiota*, and *Campilobacterota* were decreased (Fig. 5F).

3.4. Cell viability assay in HepG2/CaCO2 cells

To further investigate effects of YSHS on gut-liver axis-modulated lipid metabolism in DN animals, cell lines including HepG₂ and CaCO₂ were applied. As low-grade inflammation and high insulin are two characteristics, we firstly stimulated cells with insulin and

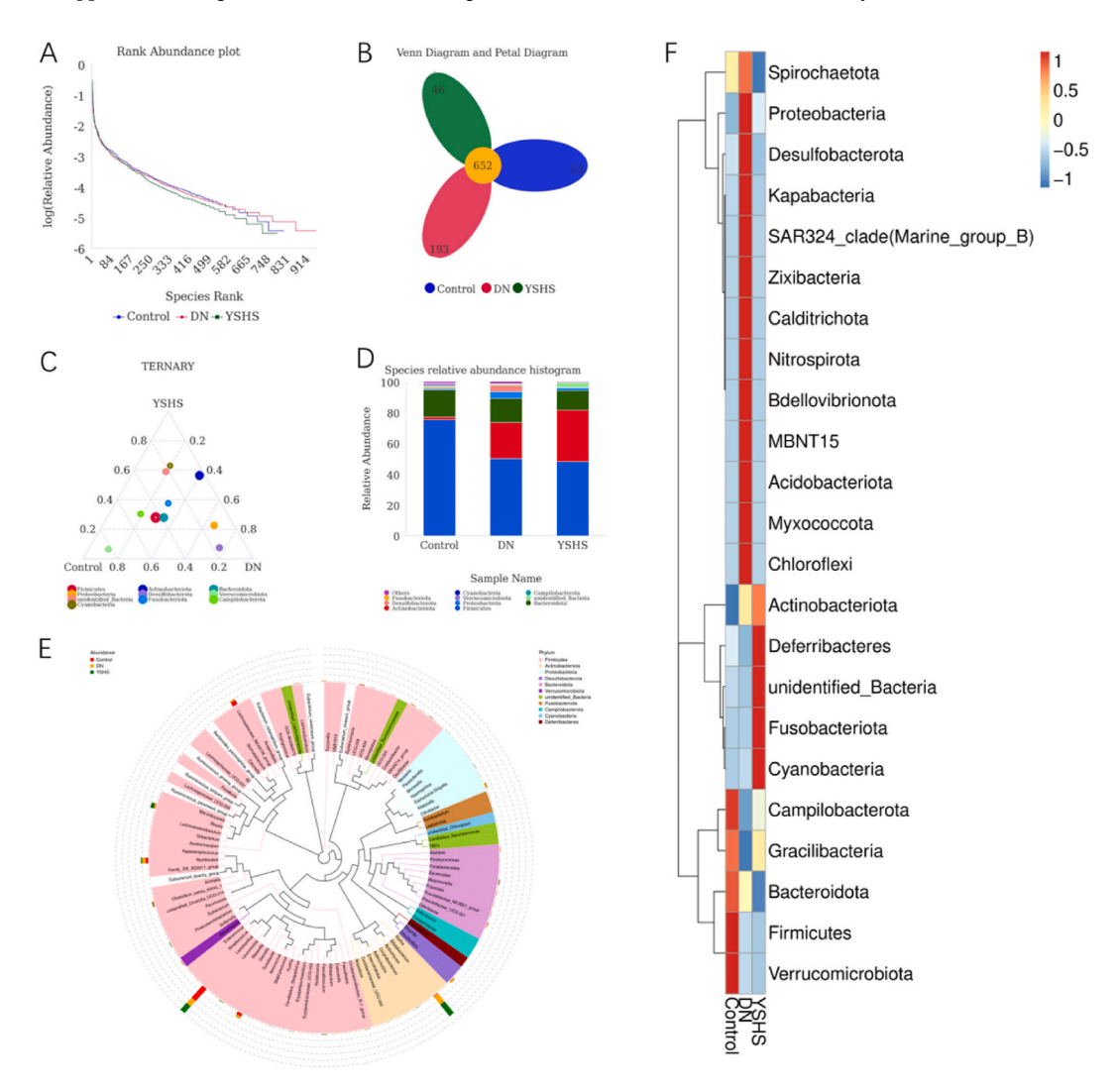


Fig. 5. YSHS ameliorated intestinal microbiota composition in DN rats. Rank abundance plot (A); venn diagram and petal diagram (B); ternary phase diagram (C); species relative abundance column chart (D); genus-level species tree (E); species abundance cluster heatmap (F).

lipopolysaccharides (LPS). As indicated by the CCK8 assay, insulin had a cytotoxic effect in a wide range of $0.1-100~\mu M$ (Fig. 6A, D) in both cells, and we chose $1~\mu M$ for following stimuli; LPS decreased CaCO₂ cell viability in the range of $1~\mu g/mL \sim 10~mg/mL$ (Fig. 6B), but it had more destructive effect in HepG₂ cells (Fig. 6E), finally we applied $1~\mu g/mL$ (HepG₂) or $100~\mu g/mL$ (CaCO₂) of LPS in the following study. To preliminary observe effects of YSHS on cell viability, HepG₂ or CaCO₂ cells were incubated with YSHS at concentrations ranging from 1-10~mg/mL under high-insulin and LPS circumstance, we found YSHS significantly restored the cell viability. Finally, YSHS was used at 1~mg/mL in CaCO₂ and 2.5~mg/mL in HepG₂ cells (Fig. 6C, F).

3.5. The intervention of YSHS repaired the intestine barrier in CaCO₂ cells

As YSHS modulated intestinal ultra-structure as observed by TEM (Fig. 3D). To further clarify if YSHS could preserve the intestinal barrier, we used WB to measure the expression of tight-junction (TJ) proteins in CaCO₂ cells. As shown in Fig. 7, exposure to insulin/LPS inhibited the expression of VE-cadherin (VE), ZO-1, Occludin, and Claudin-5, and induced a so-called "gut-leak" (Fig. 7A–D); while the expression of TJ protein was markedly increased by YSHS (Fig. 7E–H). Converging with findings in TEM (Fig. 3D), YSHS enhanced integrity of intestinal barrier.

3.5.1. YSHS modulated lipid metabolism in $HepG_2$ cells

To evaluate direct effect of YSHS on hepatocytes, $HepG_2$ cells were incubated with drugs. As shown in Fig. 8 A-F, there was a significant decrease of AST, LDL-C, TC and TG, while increase of HDL-C levels after drug administration (Fig. 8A–F).

3.5.2. YSHS modulated autophagy and inhibited mTOR/AMPK/PI3K/AKT signaling pathway in HepG2 cells

Autophagy has been recently demonstrated to modulate lipid metabolism within hepatocytes [24] and mitochondrial function plays a pivotal in this modulation [25]. In the present study, we found YSHS significantly inhibited expression of LC3B (Fig. 9A–E), LC3B-II/LC3B–I indicates the level of autophagy, in our present study, the level of autophagy was significantly increased by YSHS (Fig. 9F). Moreover, Mitochondrial DNA copy number in HepG₂ cells was increased (Fig. 9G).

To further investigate potential mechanism, related intracellular signaling pathways were studied. By both WB and immunofluorescence method, we found YSHS treatment significantly inhibited activation and expression of mTOR/AMPK/PI3K/AKT pathway proteins in HepG2 cells (Fig. 10A–J).

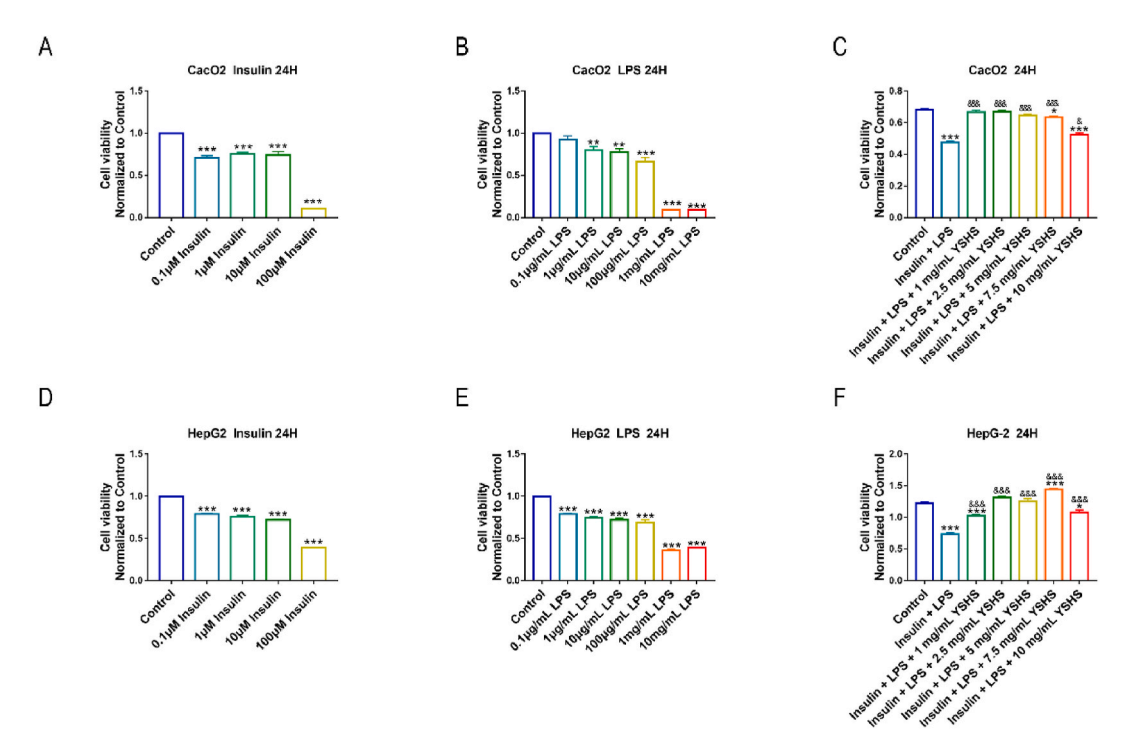


Fig. 6. $HepG_2/CaCO_2$ cells viability assay. (A) Insulin, (B) LPS, and (C) YSHS concentrated-dependently inhibited $CaCO_2$ cell viability. (D) Insulin, (E) LPS, and (F) YSHS concentrated-dependently inhibited $HepG_2$ cell viability, *p < 0.05, **p < 0.01, ***p < 0.001, vs. Control. *p < 0.05, **p < 0.01, ***p < 0.001, vs. Insulin + LPS.

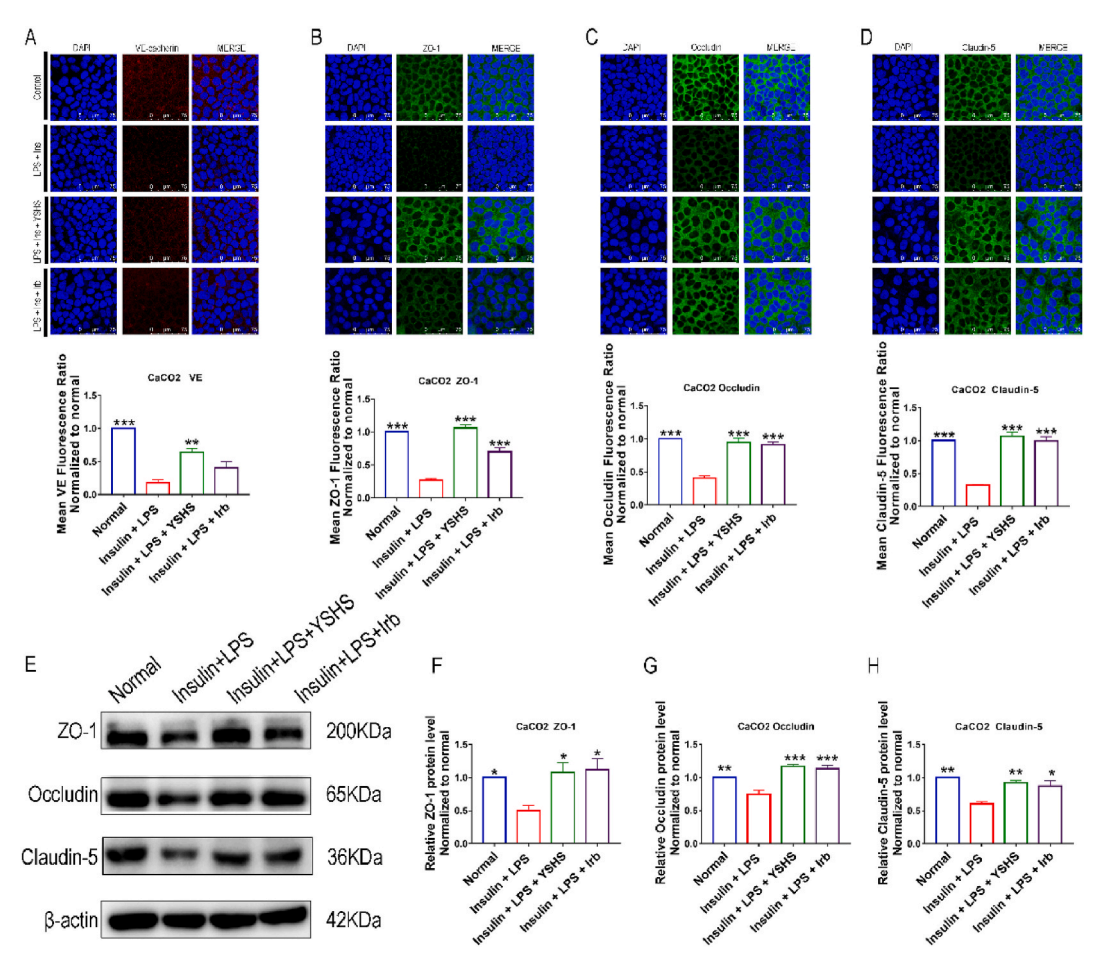


Fig. 7. YSHS repaired the intestine barrier integrity in $CaCO_2$ cells. Expressions of VE (A), ZO-1 (B), Occludin (C), and Claudin-5 (D) were determined by immunofluorescence assay under laser scanning confocal microscope. Relative fluorescence intensities of the tight junction proteins were determined by Image-J software. WB detection (E) for ZO-1, Occludin, and Claudin-5 proteins expression and quantitative analysis of ZO-1 (F), Occludin (G), and Claudin-5 (H). *p < 0.05, **p < 0.01, ***p < 0.001, vs. Insulin + LPS.

4. Discussion

Diabetic nephropathy (DN) is often considered to be a consequence of hyperglycemia in a setting of diabetes mellitus. Lipid dysmetabolism is one of the main features of diabetes mellitus and manifests by dyslipidemia as well as the ectopic accumulation of lipids in various tissues and organs, including the kidney [26]. Studies [27,28] suggest that impaired cholesterol metabolism, increased lipid uptake or synthesis, increased fatty acid oxidation, lipid droplet accumulation and an imbalance in biologically active sphingolipids (such as ceramide, ceramide-1-phosphate and sphingosine-1-phosphate) contribute to the development of DN. Currently, the literature suggests that both quality and quantity of lipids are associated with DN and contribute to increased reactive oxygen species (ROS) production, oxidative stress, inflammation, or cell death. In the present study, we found a chinese herbal formula YSHS ameliorates lipid accumulating in DN via modulating gut-liver axis.

There is *in vivo* study suggests that DN always contributes to lipotoxicity, and lipid levels are associated with the gut microbiota composition [29], these results demonstrated that the "gut-liver axis" is exerted to maintain the homeostasis of the gut microbiota and regulate liver lipid metabolism [30]. As an important part of the intestinal mucosal biological barrier, the intestinal microecology protects the intestinal tract from the invasion of pathogenic bacteria and assists nutrient absorption. Intestinal dysbiosis is involved in a variety of chronic diseases, such as diabetes and cardiovascular disease. The intestinal epithelial barrier plays an essential role in maintaining intestinal homeostasis. Destruction of intestinal barrier will significantly increase intestinal permeability and finally makes intestinal bacteria easy to *trans*-locate through the barrier to visceral organs [31]. Previously, we have demonstrated that metabolites from gut microbiota short chain fatty acids protected against liver and kidney damage under diabetic setting [13,32,33]; furthermore, short chain fatty acids preserved gut integrity in diabetic mice [9]. Across animal and human studies with chronic kidney disease, the proportion of *Bactemides* and *Lactobacillus* [34] was reduced. Furthermore, in chronic kidney disease patients, the proportion of *Prevotella* [35,36], *Ruminococcaceae*, *Roseburia*, *Faecalibacterium* [35] has decreased while the proportion of *Parabacteroides* [36], *Enterobacteriaceae* [36] and *Klebsiella* [35] has increased. In the present study, we found YSHS significantly

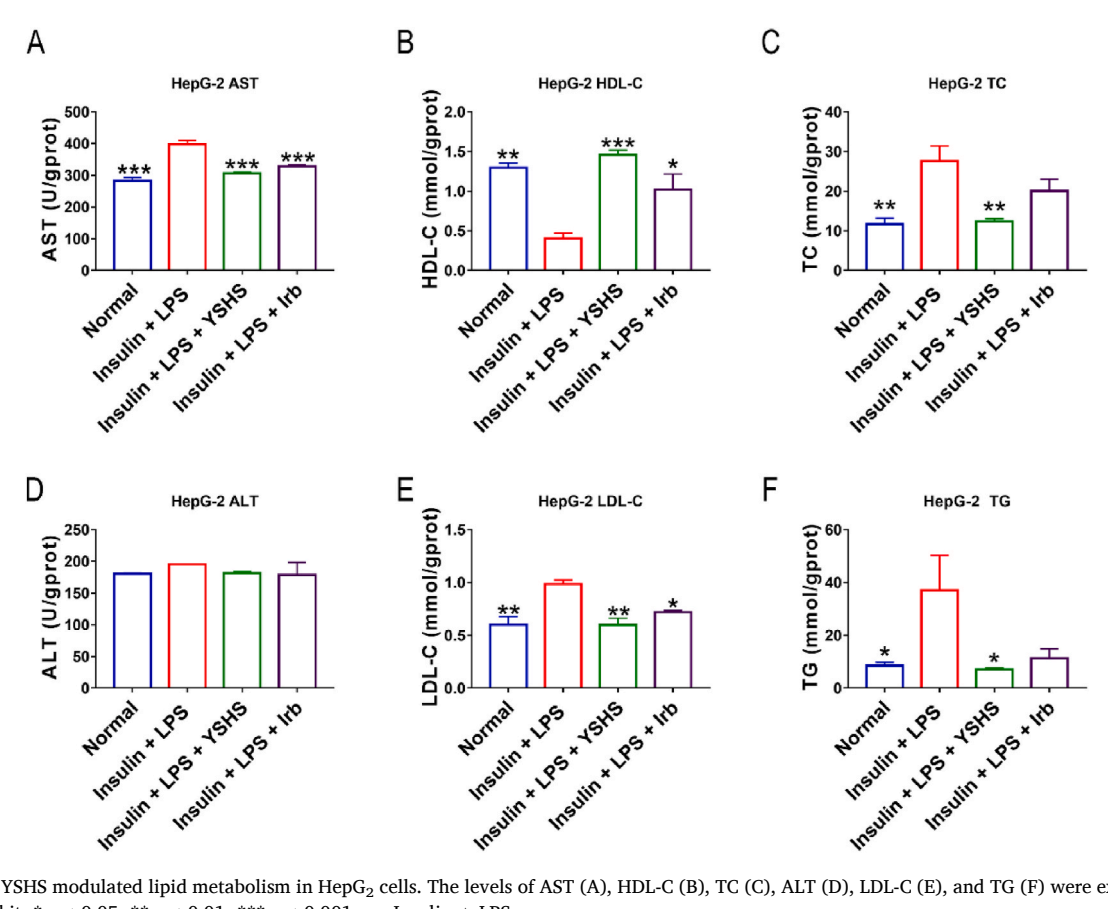


Fig. 8. YSHS modulated lipid metabolism in HepG2 cells. The levels of AST (A), HDL-C (B), TC (C), ALT (D), LDL-C (E), and TG (F) were examined by EIA kit. *p < 0.05, **p < 0.01, ***p < 0.001, vs. Insulin + LPS.

enriched composition of gut flora and increased integrity of intestinal barrier. This effects obviously inhibited the translocation of gut bacteria as well as its derived LPS into systemic circulation.

The main pathogenic basis of pre-DN is the disorder of glucose and lipid metabolism caused by insulin resistance, which leads to the lesions of the liver [37]. DN is accompanied with liver damage, and YSHS administration can significantly reduce the content of ALT, AST, TC, TG, LDL-C, increase the level of HDL-C; our finding also indicated that YSHS may ameliorate insulin resistance and metabolism disorder via modulating lipid metabolism [37]. Our present findings are also in accordance with previous report that protecting liver function can effectively delay the progress of diabetes and its complications [13].

Mitochondria plays a central role in modulating metabolism within cells [38,39]. In the present study, we observed that YSHS elevated mitochondrial DNA copy number, indicating mitochondrial biogenesis was increased. Beside this, the decrease in PGC-1α was largely counteracted by YSHS. PGC-1α is a substrate of Sirt1 [40]. AMPK is upstream regulatory factors of PGC-1α. Report from Bai and colleagues indicated that there may be an internal relationship among them [41]. Therefore, we also analyzed AMPK expression and our data showed that AMPK was increased by LPS and insulin treatment, and this trend was also modulated by YSHS.

PI3K/Akt/mTOR is a classic signaling pathway found to be highly expressed in DN, and the blockade of these pathways may slow the progression and development of DN [21]. In order to study whether they are related to the inhibition effects of YSHS on lipid metabolism in DN, both in vitro and in vivo studies were carried out. We found YSHS significantly decreased PI3K/Akt/mTOR expression and phosphorylation.

This study has limitations that should be acknowledged. For instance, there were no serological indicators associated with diabetic nephropathy detected in the study, which may limit its generalizability. It will be possible to apply in future studies with a larger sample and more serological indicators. Moreover, due to time constraints, our study focuses only on PI3K/AKT/mTOR signaling pathways, thus limiting the findings. In the future, investigations with altered gut bacteria will allow for a more comprehensive analysis of the role of YSHS to be assessed.

In conclusion, we found in this study that YSHS modulated lipid metabolism in DN via gut-liver axis, and PI3K/AKT/mTOR signaling pathway participated in this process (Fig. 11). Our finding will bring new idea of pivotal role of gut-liver axis in intervening diabetic complication, and will also help to understand mechanism of YSHS on treating DN.

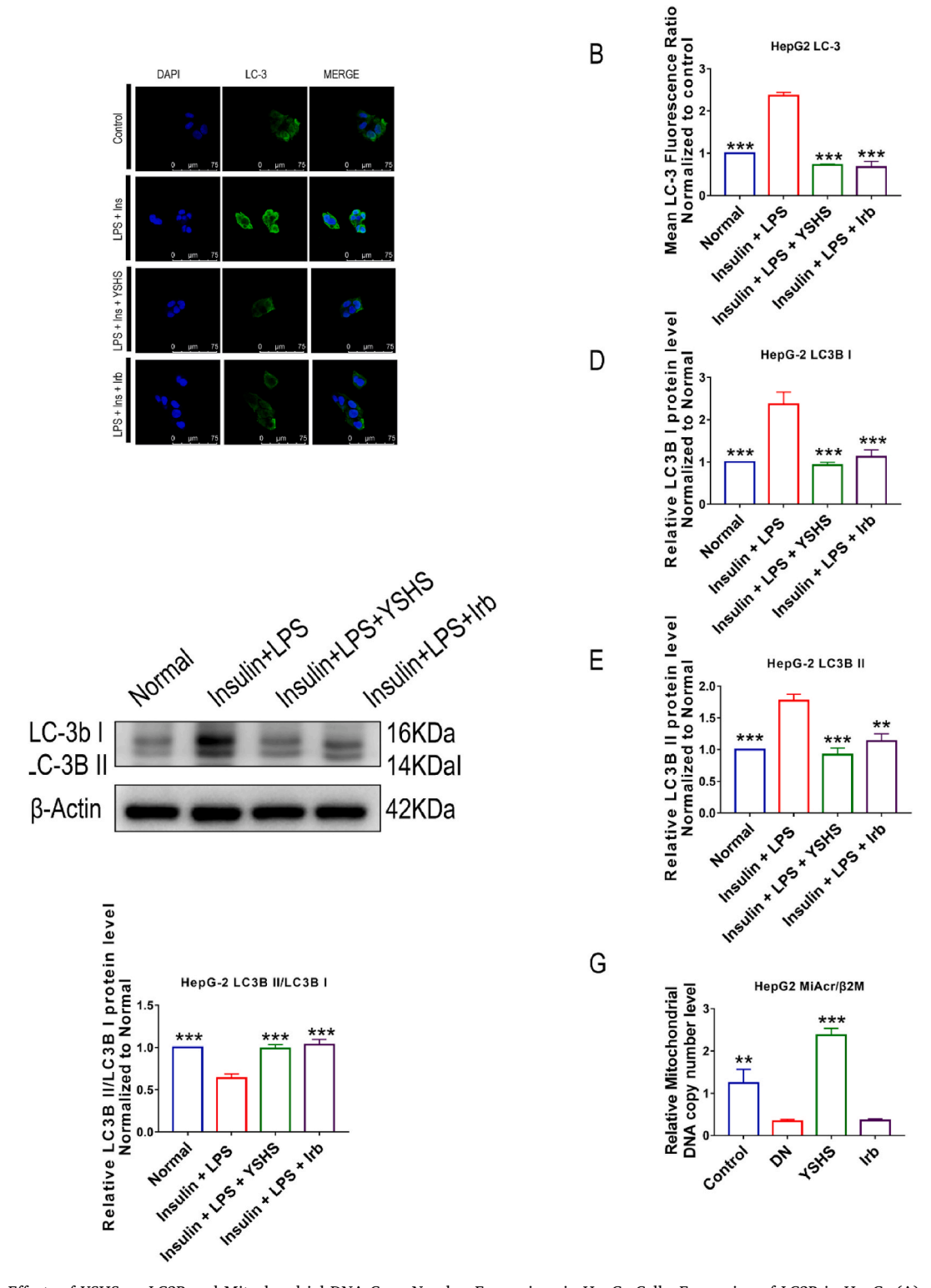


Fig. 9. Effects of YSHS on LC3B and Mitochondrial DNA Copy Number Expressions in HepG $_2$ Cells. Expression of LC3B in HepG $_2$ (A) cells was determined by immunofluorescence assay under laser scanning confocal microscope; relative fluorescence intensities of the proteins(B) were determined by Image-J software. Expression of LC3B and β-actin (C) were determined by Western Blot, and ratio were assayed by Image J software (D–F). Expressions of mitochondrial DNA copy number (G) in HepG $_2$ cells were analyzed by Q-PCR. *p < 0.05, **p < 0.01, ***p < 0.001, vs. Insulin + LPS.

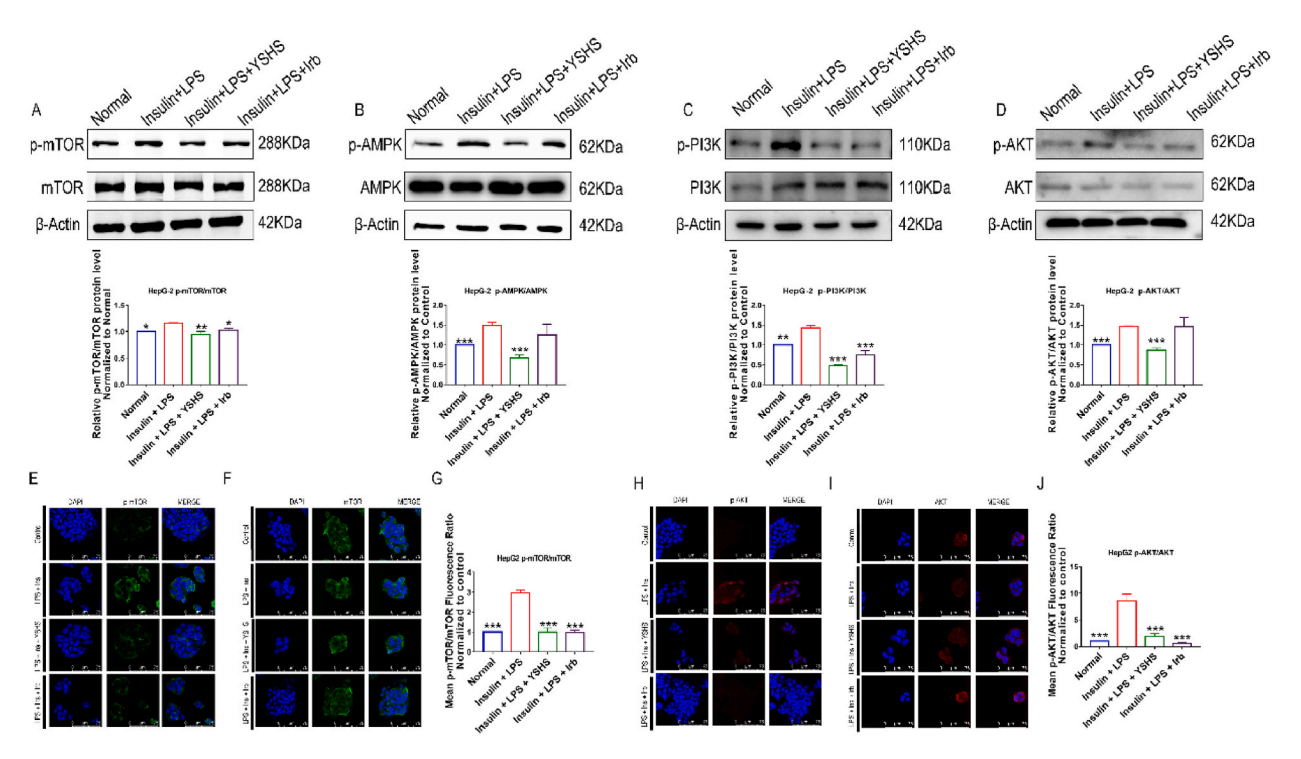


Fig. 10. YSHS regulated lipid metabolism injury in HepG₂ via PI3K/AKT/mTOR pathway. Expression of p-mTOR (A), mTOR (A), p-AMPK (B), AMPK (B), p-PI3K (C), PI3K (C), p-AKT (D), and AKT (D) were determined by Western Blot, ratio was assayed by Image J software. Expressions of p-mTOR (E), mTOR (F) p-AKT (H), and AKT (I) was determined by immunofluorescence assay under laser scanning confocal microscope. Relative fluorescence intensities of the ratio of p-mTOR/mTOR (G) and the ratio of p-AKT/AKT (J) were determined by Image-J software. *p < 0.05, **p < 0.01, ***p < 0.001, vs. Insulin + LPS.

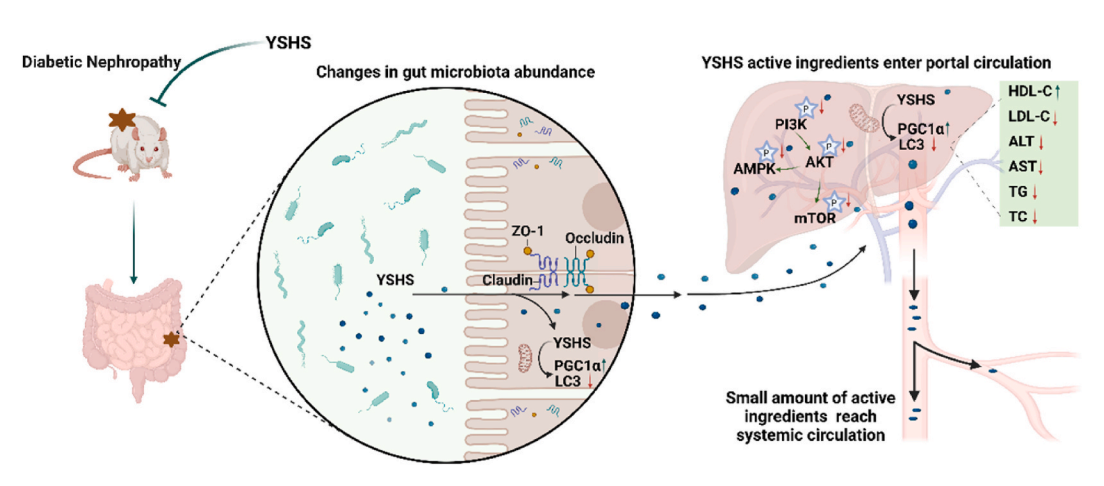


Fig. 11. A schematic presentation for the possible mechanisms of YSHS on modulating gut-liver axis and preventing diabetic damage.

Author contribution statement

Tingting Zhao, Qian Xiang: Performed the experiments; Analyzed and interpreted the data; Wrote the paper.

Beifeng Lie: Performed the experiments; Analyzed and interpreted the data.

Deqi Chen, Minyi Li, Xi Zhang, Ruixue Dong: Performed the experiments.

Junzheng YangORCID, Bao He, Wei Zhang: Contributed reagents, materials, analysis tools or data.

Yadi Liu, Junling Gu, Yijing Yao: Analyzed and interpreted the data.

Quan Zhu, Tingting Duan, Zhenghai Li: Conceived and designed the experiments.

Youhua Xu: Conceived and designed the experiments; Wrote the paper.

Funding statement

Youhua Xu was supported by Science and Technology Development Fund of Macau [0025/2019/AGJ & 0055/2019/AMJ]. Zhenghai Li was supported by Department of Science and Technology of Guangdong Province [2020A050515013].

Data availability statement

Data will be made available on request.

Declaration of interest's statement

The authors declare that they have no known competing financial interests or personal relationships that could have appeared to influence the work reported in this paper.

Abbreviations

DN	Diabetic nephropathy			
YSHS	Yishen Huashi granules			
CT7	Strontozotocin			

STZ Streptozotocin IRB Irbesartan

AST Aspartate transaminase
ALT Alanine transaminase
LDL Low-density lipoprotein
HDL High-density lipoprotein
YSHS Yishen Huashi granules
LDL Low-density lipoprotein
HDL High-density lipoprotein

 $PGC1\alpha$ Co-activator- 1α SIRT1 Sirtuin 1 LC3 Light Chain 3

mTOR Mammalian target of rapamycin AMPK AMP-activated protein kinase PI3K Phosphoinositide 3-kinase

AKT Protein kinase B
PAS Periodic acid–Schiff

TEM Transmission electron microscopy

PCR Polymerase chain reaction

CCK8 Cell counting kit-8
FBS Fetal bovine serum
PS Penicillin-streptomycin
BAX Bcl-2-associated X protein
ZO-1 Zona occludens 1

TC Total cholesterolTG TriglycerideLPS Lipopolysaccharides

Appendix A. Supplementary data

Supplementary data to this article can be found online at https://doi.org/10.1016/j.heliyon.2023.e14171.

References

- [1] R. Saran, B. Robinson, K.C. Abbott, et al., US renal data System 2017 annual data report: epidemiology of kidney disease in the United States, Am. J. Kidney Dis. 71 (2018) A7, https://doi.org/10.1053/j.ajkd.2018.01.002.
- [2] A. Lim, Diabetic nephropathy complications and treatment, Int. J. Nephrol. Renovascular Dis. 7 (2014) 361–381, https://doi.org/10.2147/JJNRD.S40172.
- [3] R. Dentin, F. Benhamed, I. Hainault, et al., Liver-specific inhibition of ChREBP improves hepatic steatosis and insulin resistance in ob/ob mice, Diabetes 55 (2006) 2159–2170, https://doi.org/10.2337/db06-0200.
- [4] D.B. Savage, C.S. Choi, V.T. Samuel, et al., Reversal of diet-induced hepatic steatosis and hepatic insulin resistance by antisense oligonucleotide inhibitors of acetyl-CoA carboxylases 1 and 2, J. Clin. Invest. 116 (2006) 817–824, https://doi.org/10.1172/JCI27300.

[5] A. Seppala-Lindroos, S. Vehkavaara, A.M. Hakkinen, et al., Fat accumulation in the liver is associated with defects in insulin suppression of glucose production and serum free fatty acids independent of obesity in normal men, J. Clin. Endocrinol. Metab. 87 (2002) 3023–3028, https://doi.org/10.1210/jcem.87.7.8638.

- [6] M.P. Mollica, G. Mattace Raso, G. Cavaliere, et al., Butyrate regulates liver mitochondrial function, efficiency, and dynamics in insulin-resistant obese mice, Diabetes 66 (2017) 1405–1418, https://doi.org/10.2337/db16-0924.
- [7] L. Belloni, S. Di Cocco, F. Guerrieri, et al., Targeting a phospho-STAT3-miRNAs pathway improves vesicular hepatic steatosis in an in vitro and in vivo model, Sci. Rep. 8 (2018), 13638, https://doi.org/10.1038/s41598-018-31835-2.
- [8] R.A. Haeusler, T.E. McGraw, D. Accili, Biochemical and cellular properties of insulin receptor signalling, Nat. Rev. Mol. Cell Biol. 19 (2018) 31–44, https://doi.org/10.1038/nrm.2017.89
- [9] Y.H. Xu, C.L. Gao, H.L. Guo, et al., Sodium butyrate supplementation ameliorates diabetic inflammation in db/db mice, J. Endocrinol. 238 (2018) 231–244, https://doi.org/10.1530/JOE-18-0137
- [10] Q. Zhang, H. Yu, X. Xiao, et al., Inulin-type fructan improves diabetic phenotype and gut microbiota profiles in rats, PeerJ 6 (2018) e4446, https://doi.org/
- [11] Q. Ma, Y. Li, P. Li, et al., Research progress in the relationship between type 2 diabetes mellitus and intestinal flora, Biomed. Pharmacother. 117 (2019), 109138, https://doi.org/10.1016/j.biopha.2019.109138.
- [12] W. Jia, G. Xie, W. Jia, Bile acid-microbiota crosstalk in gastrointestinal inflammation and carcinogenesis, Nat. Rev. Gastroenterol. Hepatol. 15 (2018) 111–128, https://doi.org/10.1038/nrgastro.2017.119.
- [13] W.Q. Zhang, T.T. Zhao, D.K. Gui, et al., Sodium butyrate improves liver glycogen metabolism in type 2 diabetes mellitus, J. Agric. Food Chem. 67 (2019) 7694–7705, https://doi.org/10.1021/acs.jafc.9b02083.
- [14] X. Li, T. Zhao, J. Gu, et al., Intake of flavonoids from Astragalus membranaceus ameliorated brain impairment in diabetic mice via modulating brain-gut axis, Chin. Med. 17 (2022) 22, https://doi.org/10.1186/s13020-022-00578-8.
- [15] Y. Xu, L. Feng, S. Wang, et al., Calycosin protects HUVECs from advanced glycation end products-induced macrophage infiltration, J. Ethnopharmacol. 137 (2011) 359–370, https://doi.org/10.1016/j.jep.2011.05.041.
- [16] T. Zhu, H. Wang, L. Wang, et al., Ginsenoside Rg1 attenuates high glucose-induced endothelial barrier dysfunction in human umbilical vein endothelial cells by protecting the endothelial glycocalyx, Exp. Ther. Med. 17 (2019) 3727–3733, https://doi.org/10.3892/etm.2019.7378.
- [17] Y. Xu, J. Xiong, Y. Zhao, et al., Calycosin rebalances advanced glycation end products-induced glucose uptake dysfunction of hepatocyte in vitro, Am. J. Chin. Med. 43 (2015) 1191–1210, https://doi.org/10.1142/S0192415X15500688.
- [18] T. P. o. Y. H. i. C. A. o. C. Medicine, The panel of Yishen Huashi in China association of Chinese medicine. Expert consensus of Yishen Huashi granule on kidney disease, Chin. J. Kidney Dis. Invest. (Electronic Edition) 9 (3) (2020) 97–101.
- [19] N. Papadopoulou-Marketou, S.A. Paschou, N. Marketos, et al., Diabetic nephropathy in type 1 diabetes, Minerva Med. 109 (2018) 218–228, https://doi.org/
- [20] T. Zhao, M. Li, Q. Xiang, et al., Yishen Huashi granules ameliorated the development of diabetic nephropathy by reducing the damage of glomerular filtration barrier, Front. Pharmacol. 13 (2022), 872940, https://doi.org/10.3389/fphar.2022.872940.
- [21] W. Wu, W. Hu, W.B. Han, et al., Inhibition of akt/mTOR/p7086K signaling activity with Huangkui capsule alleviates the early glomerular pathological changes in diabetic nephropathy, Front. Pharmacol. 9 (2018) 443, https://doi.org/10.3389/fphar.2018.00443.
- [22] The Pharmacopoeia of the People's Republic of China, China Medical Science Press, Beijing, 2020.
- [23] N.R. Phillips, M.L. Sprouse, R.K. Roby, Simultaneous quantification of mitochondrial DNA copy number and deletion ratio: a multiplex real-time PCR assay, Sci. Rep. 4 (2014) 3887, https://doi.org/10.1038/srep03887.
- [24] Y.H. Chen, T.Y. Huang, Y.T. Lin, et al., VPS34 K29/K48 branched ubiquitination governed by UBE3C and TRABID regulates autophagy, proteostasis and liver metabolism, Nat. Commun. 12 (2021) 1322, https://doi.org/10.1038/s41467-021-21715-1.
- [25] G. Biczo, E.T. Vegh, N. Shalbueva, et al., Mitochondrial dysfunction, through impaired autophagy, leads to endoplasmic reticulum stress, deregulated lipid metabolism, and pancreatitis in animal models. Gastroenterology 154 (2018) 689–703, https://doi.org/10.1053/j.gastro.2017.10.012.
- [26] A. Mitrofanova, G. Burke, S. Merscher, et al., New insights into renal lipid dysmetabolism in diabetic kidney disease, World J. Diabetes 12 (2021) 524–540, https://doi.org/10.4239/wjd.v12.i5.524.
- https://doi.org/10.4259/wjd.v12.15.324. [27] A. Mitrofanova, A.M. Fontanella, S. Merscher, et al., Lipid deposition and metaflammation in diabetic kidney disease, Curr. Opin. Pharmacol. 55 (2020) 60–72, https://doi.org/10.1016/j.coph.2020.09.004.
- [28] G.M. Ducasa, A. Mitrofanova, A. Fornoni, Crosstalk between lipids and mitochondria in diabetic kidney disease, Curr. Diabetes Rep. 19 (2019) 144, https://doi.org/10.1007/s11892-019-1263-x.
- [29] M. Schoeler, R. Caesar, Dietary lipids, gut microbiota and lipid metabolism, Rev. Endocr. Metab. Disord. 20 (2019) 461–472, https://doi.org/10.1007/s11154-019.09512.0
- [30] P. Li, K. Yan, X. Chang, et al., Sex-specific maternal calcium requirements for the prevention of nonalcoholic fatty liver disease by altering the intestinal microbiota and lipid metabolism in the high-fat-diet-fed offspring mice, Gut Microb. 11 (2020) 1590–1607, https://doi.org/10.1080/19490976.2020.1768645.
- [31] X. Zhang, Q. Zhao, C. Wu, et al., Nitrate is crucial for the proliferation of gut Escherichia coli caused by H9N2 AIV infection and effective regulation by Chinese herbal medicine ageratum-liquid, Front. Microbiol. 11 (2020), 555739, https://doi.org/10.3389/fmicb.2020.555739.
- [32] W. Huang, Y. Man, C. Gao, et al., Short-chain fatty acids ameliorate diabetic nephropathy via GPR43-mediated inhibition of oxidative stress and NF-kappaB signaling, Oxid. Med. Cell. Longev. 2020 (2020), 4074832, https://doi.org/10.1155/2020/4074832.
- [33] T. Zhao, J. Gu, H. Zhang, et al., Sodium butyrate-modulated mitochondrial function in high-insulin induced HepG2 cell dysfunction, Oxid. Med. Cell. Longev. 2020 (2020), 1904609, https://doi.org/10.1155/2020/1904609.
- [34] A. Leyva-Soto, R. Alejandra Chavez-Santoscoy, O. Porras, et al., Epicatechin and quercetin exhibit in vitro antioxidant effect, improve biochemical parameters related to metabolic syndrome, and decrease cellular genotoxicity in humans, Food Res. Int. 142 (2021), 110101, https://doi.org/10.1016/j. foodres.2020.110101.
- [35] S. Jiang, S. Xie, D. Lv, et al., Alteration of the gut microbiota in Chinese population with chronic kidney disease, Sci. Rep. 7 (2017) 2870, https://doi.org/ 10.1038/s41598-017-02989-2
- [36] K.Y. Xu, G.H. Xia, J.Q. Lu, et al., Impaired renal function and dysbiosis of gut microbiota contribute to increased trimethylamine-N-oxide in chronic kidney disease patients, Sci. Rep. 7 (2017) 1445, https://doi.org/10.1038/s41598-017-01387-y.
- [37] Y. Ding, X. Xian, W.L. Holland, et al., Low-density lipoprotein receptor-related protein-1 protects against hepatic insulin resistance and hepatic steatosis, EBioMedicine 7 (2016) 135–145, https://doi.org/10.1016/j.ebiom.2016.04.002.
- [38] H. Wang, C. Liu, Y. Zhao, et al., Mitochondria regulation in ferroptosis, Eur. J. Cell Biol. 99 (2020), 151058, https://doi.org/10.1016/j.ejcb.2019.151058.
- [39] L. Sedlackova, V.I. Korolchuk, Mitochondrial quality control as a key determinant of cell survival, Biochim. Biophys. Acta Mol. Cell Res. 1866 (2019) 575–587, https://doi.org/10.1016/j.bbancr.2018.12.012.
- [40] J.T. Rodgers, C. Lerin, W. Haas, et al., Nutrient control of glucose homeostasis through a complex of PGC-1alpha and SIRT1, Nature 434 (2005) 113–118, https://doi.org/10.1038/nature03354.
- [41] Y. Bai, J. Zuo, X. Fang, et al., Protective effect of Jiang Tang Xiao Ke granules against Skeletal muscle IR via activation of the AMPK/SIRT1/PGC-1alpha signaling pathway, Oxid. Med. Cell. Longev. 2021 (2021), 5566053, https://doi.org/10.1155/2021/5566053.